International Journal of Nanomedicine

Dovepress
open access to scientific and medical research

Open Access Full Text Article

ORIGINAL RESEARCH

Magnetic and fluorescent Gd_2O_3:Yb^{3+}/Ln^{3+} nanoparticles for simultaneous upconversion luminescence/MR dual modal imaging and NIR-induced photodynamic therapy

This article was published in the following Dove Press journal:
International Journal of Nanomedicine
16 December 2016
Number of times this article has been viewed

Jun Liu,[1,*] Long Huang,[2,3,*] Xiumei Tian,[4] Xiaoming Chen,[4] Yuanzhi Shao,[5] Fukang Xie,[3] Dihu Chen,[1] Li Li[2]

[1]School of Electronics and Information Technology and School of Physics, [2]State Key Laboratory of Oncology in South China, Imaging Diagnosis and Interventional Center, [3]Department of Histology and Embryology, Zhongshan School of Medicine, Sun Yat-Sen University, [4]Department of Biomedical Engineering, Guangzhou Medical University, [5]State Key Laboratory of Optoelectronic Materials and Technologies, Sun Yat-Sen University, Guangzhou, People's Republic of China

*These authors contributed equally to this work

Correspondence: Dihu Chen
School of Electronics and Information Technology and School of Physics, Sun Yat-Sen University, Guangzhou 510060, People's Republic of China
Tel +86 20 136 0045 2080
Fax +86 20 8411 3398
Email stscdh@mail.sysu.edu.cn

Li Li
State Key Laboratory of Oncology in South China, Imaging Diagnosis and Interventional Center, Sun Yat-Sen University, Guangzhou 510275, People's Republic of China
Tel +86 20 8734 3476
Fax +86 20 8734 3476
Email li2@mail.sysu.edu.cn

Abstract: The development of upconversion nanoparticles (UCNs) for theranostics application is a new strategy toward the accurate diagnosis and efficient treatment of cancer. Here, magnetic and fluorescent lanthanide-doped gadolinium oxide (Gd_2O_3) UCNs with bright upconversion luminescence (UCL) and high longitudinal relaxivity (r_1) are used for simultaneous magnetic resonance imaging (MRI)/UCL dual-modal imaging and photodynamic therapy (PDT). In vitro and in vivo MRI studies show that these products can serve as good MRI contrast agents. The bright upconversion luminescence of the products allows their use as fluorescence nanoprobes for live cells imaging. We also utilized the luminescence-emission capability of the UCNs for the activation of a photosensitizer to achieve significant PDT results. To the best of our knowledge, this study is the first use of lanthanide-doped Gd_2O_3 UCNs in a theranostics application. This investigation provides a useful platform for the development of Gd_2O_3-based UCNs for clinical diagnosis, treatment, and imaging-guided therapy of cancer.

Keywords: upconversion nanoparticles, upconversion luminescence imaging, MR imaging, photodynamic therapy, singlet oxygen

Introduction

Cancer is still one of the most devastating human diseases, causing millions of deaths every year. Accurate diagnosis and efficient treatment of cancer are crucially important to increase the survival rate of patients. However, current diagnostic and therapeutic techniques are still far from satisfaction. Photodynamic therapy (PDT) is considered to be an effective technique for cancer treatment because it is cost-effective, highly localized, and has fewer side effects compared to radiation therapy and chemotherapy.[1–3] It involves local or systemic administration of a photosensitizer (PS), followed by irradiation of the target lesion with light of a specific wavelength. This triggers oxidative photodamage by the generation of reactive oxygen species, especially singlet oxygen, subsequently leading to tumor cell killing.[4] However, most of the currently available PSs are activated by visible light (400–700 nm), which has a limited penetration depth in biological tissues. In contrast, the near-infrared (NIR) within the "optical transparency window" (700–1,100 nm) of biological tissues not only results in low photodamage but also possesses high tissue penetration capability.[5–7] A novel strategy of combining the PS with lanthanide-doped upconversion nanoparticles (UCNs) can overcome the previous limitations and has recently attracted interest in the field of malignant tumor

submit your manuscript | www.dovepress.com
Dovepress
http://dx.doi.org/10.2147/IJN.S118938

therapy. In this novel system, UCNs activate the PS by visible light emission generated from sequential multiphoton NIR excitation via an anti-Stokes process.[8–10]

In 2007, Zhang et al first reported the use of $NaYF_4$:Yb^{3+}/Er^{3+} UCNs for PDT application.[11] Since then, the UCNs have been used for PDT by many groups.[12–14] Both the dopants and host of UCNs are important to achieve efficient PDT. There are two types of dopants ions in UCNs: a sensitizer to absorb the NIR light and an activator to emit photons and further activate the PS. The Yb^{3+} ion is the most commonly used sensitizer ion because its $^2F_{7/2} \rightarrow {}^2F_{5/2}$ transition has a large absorption cross-section around 980 nm. The Er^{3+} ion is a highly efficient activator because many of its f-f transitions resonant well with the $^2F_{7/2} \rightarrow {}^2F_{5/2}$ transition of Yb^{3+}. For effective PDT, the choice of the UCNs host is critical for obtaining good upconversion efficiency. A popular host material is $NaYF_4$, which exhibits high upconversion efficiency due to the low phonon cutoff energy,[15] thus attracting much interest in UCNs-based PDT and upconversion luminescence (UCL) imaging.[16–19] Other fluorides containing Yb^{3+} ($NaYbF_4$) and Gd^{3+} ($NaGdF_4$) ions, which also function as computed tomography (CT) and magnetic resonance imaging (MRI) contrast agents,[20–24] have been utilized to achieve simultaneous dual- or multimodal bioimaging with high sensitivity and high spatial resolution. These multifunctional nanoparticles can satisfy the high efficiency and accuracy requirements of clinical cancer theranostics.

Oxides, such as Gd_2O_3, ZrO_2, and Y_2O_3, are also generally used as luminescence host materials towing to their desirable chemical durability, thermal stability, and lower phonon energy.[25–27] Among these oxides, the Gd_2O_3 nanoparticles also exhibit higher relaxivity than clinical Gd-DTPA, and have been considered as effective T_1 MR contrast agents.[28–30] Thus, the lanthanide-doped Gd_2O_3 nanoparticles have attracted attention in the dual-modal imaging. Zhou et al used the lanthanide-doped Gd_2O_3 UCNs with the size of 10–270 nm as dual-modal nanoprobes for MR/UCL imaging.[31] Liu et al reported the application of Gd_2O_3:Yb^{3+}/Er^{3+} nanorods (length of 90–150 nm and diameter of 10–25 nm) for CT/MRI/UCL multimodal imaging.[32] Our recent work has focused on the synthesis and development of ultra-small (sub-10 nm) lanthanide-doped Gd_2O_3 nanoparticles for MR/fluorescence dual-modal imaging.[33–36] However, to the best of our knowledge, the ability of lanthanide-doped Gd_2O_3 UCNs for theranostics application, which combines the diagnosis and treatment of cancer, has not previously been reported. In this contribution, the aim was to synthesis magnetic and fluorescent lanthanide-doped Gd_2O_3 UCNs and simultaneously achieve MR/UCL dual-modal imaging and PDT. This study is part of a long term to improve the accuracy or possibilities to detect (or monitor) and treat cancer with MR/UCL dual-modal imaging and PDT by utilizing the magnetic and fluorescent properties of lanthanide-doped Gd_2O_3 UCNs.

Experimental section

Preparation and characterization of the UCNs

The UCNs were prepared by a two-step method, as previously reported.[35] Analytical grade powders of Gd_2O_3, Yb_2O_3, and Ln_2O_3 (Ln = Tm, Ho, Er) in the stoichiometric ratio of 83:15:2 were used as the raw materials to fabricate targets via a solid-state reaction technique. The UCNs were prepared utilizing the laser ablation in liquid (LAL) technique, "top-down" strategy, which generates higher purity products efficiently, and has been applied to synthesizing a variety of nanomaterials.[37] A schematic diagram of the formation mechanism of UCNs by LAL is shown in Scheme 1. The process starts with the penetration of laser pulse in the liquid and arrival to the Gd_2O_3:Yb^{3+}/Ln^{3+} target surface (Scheme 1B), then followed by a high-temperature and high-pressure plasma plume containing the ablated material produced at the target/liquid interface, accompanied by the emission of a shockwave (Scheme 1C). As there is continual absorption of laser pulse by the target, the plasma plume subsequent ultrasonic adiabatic expands into surrounding liquid (Scheme 1D).[37] During the expansion, the plasma plume quickly cools down and releases energy to the deionized water, resulting in the nucleation of the Gd_2O_3:Yb^{3+}/Ln^{3+} UCNs and growth of nuclei (Scheme 1E). Meanwhile, the energy release of plasma plume to the liquid induces the generation of a cavitation bubble, which expands into the liquid.[38] During its expansion, the temperature and pressure inside the bubble decreased rapidly and cause the collapse of the bubble. During the collapse, the pressure and temperature recover to the original values, and the high energy is released by emission of a second shockwave,[38] finally the Gd_2O_3:Yb^{3+}/Ln^{3+} UCNs are formed and ejected into surrounding liquid (Scheme 1F).The ablated colloids were allowed to stand for 24 h, before the upper liquid was collected for further measurement.

The UC fluorescence spectrum of the collected upper liquid was measured at room temperature using an Edinburgh spectrofluorophotometer (FLS920, Edinburgh Instrument Ltd., Edinburgh, UK) equipped with a 980 nm NIR laser. The structure, morphology, and component of the products were characterized using an X-ray diffractometer (XRD, D-MAX2200 VPC, Tokyo, Japan), a transmission electron microscope (TEM, FEI Tecnai G2 Spirit, FEI Company,

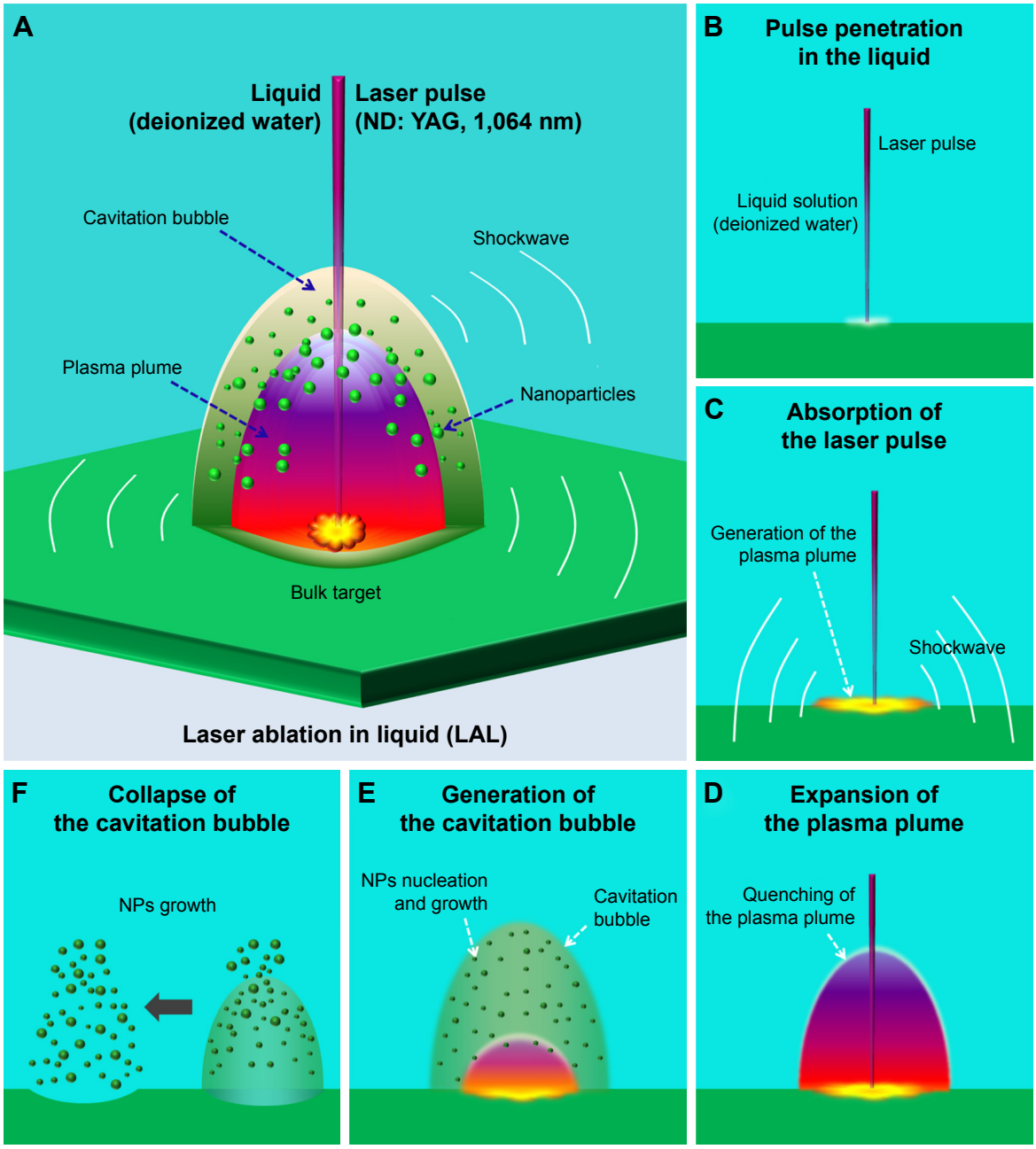

Scheme 1 Schematic illustration (**A**) and main stages (**B**–**F**) of formation mechanism of Gd_2O_3:Yb^{3+}/Ln^{3+} UCNs by LAL.
Abbreviations: LAL, laser ablation in liquid; NPs, nanoparticles; UCNs, upconversion nanoparticles.

Eindhoven, the Netherlands), and an X-ray photoelectron spectrometer (XPS, ESCALab250, Thermo Fisher Scientific, Waltham, MA, USA), respectively.

In vitro MRI measurements

In vitro T_1-weighted MRI was performed by a 3.0T Siemens Trio MRI scanner (Siemens Medical Solutions, Erlangen, Germany). The TSE T_1 axial sequence was used with the following parameters: 5% dist. factor, FOV =64 mm, slice thickness =2.0 mm, TR =600 ms, TE =12 ms, no of averages =6. In this study, various samples with Gd concentrations in the average 0–0.1 mM were measured. The signal intensities were analyzed using a picture archiving and communications system.

In vivo MRI measurements

BALB/c nude mice of 16±2 g weight were purchased from the Animal Experiment Centre of the Medical College, Sun Yat-Sen University (People's Republic of China) and housed in a pathogen-free animal facility. The study protocol was approved by the Care and Use of Laboratory Animals of Sun Yat-sen University (Permit Numbers: SCXK (Guangdong)

2011–0029). We strictly followed the Guide for the Care and Use of Laboratory Animals of Sun Yat-sen University during the study. The BALB/c nude mice were subcutaneously injected with 5×10^6 nasopharyngeal carcinoma (NPC) CNE-2 cells in 100 µL phosphate-buffered saline (PBS). Ten days after tumor cell inoculation, mice with xenografted tumor of ~60 mm^3 were anesthetized by intraperitoneal injection of 1% mebumalnatrium (10 µL/g), then injected with the Gd_2O_3:Yb^{3+}/Ln^{3+} UCNs (Gd^{3+}, 15 µmol/kg) in 100 µL of PBS (1× buffer) via the tail vein, and scanned with the 3.0-T MRI system using a 3 inch in diameter surface coil constructed specifically for small animals. To prevent bias toward aberrantly enhanced regions, normalized histograms of signal intensity were generated for the entire tumor.

Fluorescence imaging of cells

Cells from a murine macrophage cells line (RAW 264.7 cells) were cultivated under 5% CO_2 atmosphere at 37°C in Dulbecco's Modified Eagle's Medium (DMEM) containing 10% fetal bovine serum, penicillin (100 units/mL), and streptomycin (100 mg/mL). The cells were incubated with the Gd_2O_3:Yb^{3+}/Ln^{3+} UCNs (20 µg/mL) for 2 h. After co-incubation, the cells were washed with PBS to remove the remaining particles and dead cells and then observed under a laser scanning confocal microscope (LSM 710, Carl Zeiss, Jena, Germany), operating at an excitation wavelength of 980 nm.

Cytotoxicity assay

The human NPC cell lines (CNE2 cells, purchased from the Cell bank of Laboratory Animal Center, the Sun Yat-sen University Hospital, Guangzhou, People's Republic of China, with the permit number SCYK [粤] 2016-0029) were incubated with UCNs concentrations of 20, 30, 40, and 50 µg/mL in 96-well plates for 4, 6, and 8 h and compared to culture media (DMEM) as the negative control and lipopolysaccharides as the positive control. After co-incubation, 20 µL of 3-(4,5-dimethylthiazol-2-yl)-2,5-diphenyltetrazolium bromide (MTT) was added for another 4 h of incubation. The culture medium was removed and 100 µL dimethyl sulfoxide added to dissolve the formazan crystals for 10 min. The absorbance at 490 nm was measured by a microplate reader (Bio-Rad, Hercules, CA, USA).

Singlet oxygen assay

Singlet oxygen is important in PDT as the singlet oxygen kills cancer cells. The photochemical method with 1,3-diphenylisobenzofuran (DPBF) is generally used to detect singlet oxygen.[39–41] The singlet oxygen decomposes DPBF, which has an absorption wavelength of ~410 nm, thus the decreases in DPBF absorbance indicate the generation of singlet oxygen. The UCNs (Gd_2O_3:Yb^{3+}/Er^{3+}, 3.5 µg/mL, 5 µL), PS (ZnPc, 0.75 µM, 5 µL), and DPBF (10 mM, 15 µL) in solvent were irradiated with NIR light (laser diode, wavelength 980 nm, continuous wave, 0.2 W/cm^2). The DPBF absorbance was measured using a Scandrop spectrophotometer (Nanodrop 2000, Thermo Fisher Scientific, Waltham, MA, USA).

In vitro PDT

To understand the effects of PDT, the cell viability of CNE2 cells containing the UCNs and the PS was measured under NIR irradiation. The cancer cells (2×10^4 cells/100 µL) were seeded into 96-well cell culture plates. Following cultivation under dark conditions in DMEM, the cells were treated with UCNs (Gd_2O_3:Yb^{3+}/Er^{3+}, 40 µg/mL) and the PS (ZnPc, 0.75, 1.5, and 3 µM), and compared to UCNs and ZnPc control groups. All groups were cultivated under the same conditions for 4 h. The cells were washed three times with PBS and replaced into fresh culture medium. The cells were then irradiated with NIR light (laser diode, wavelength 980 nm, continuous wave, 0.2 W/cm^2). After the 30 min cultivation, the cell viability was measured by MTT assay.

Results and discussion

Upconversion fluorescence properties of the Gd_2O_3:Yb^{3+}/Ln^{3+} UCNs

The sensitizer (Yb^{3+} ions) has a much larger absorption cross-section at 980 nm and a much higher concentration than the activator (Ln^{3+} ions), thus energy transfer upconversion is the main pathway in the combined Yb^{3+}/Ln^{3+} system. Under NIR excitation at 980 nm, the Yb^{3+} ions continuously absorbed 980 nm photons and transfer the energy to the activator, resulting in photons emission. Figure 1A shows the upconversion fluorescence photograph of the collected UCNs colloids under excitation at 980 nm, as obtained by a digital camera without using any optical filters. The upconversion fluorescence colors obtained from the Yb^{3+}/Tm^{3+}, Yb^{3+}/Ho^{3+}, and Yb^{3+}/Er^{3+} combinations are blue, green, and red, respectively, which are naked-eye compatible and reflect the entire spectrum. Figure 1B shows their corresponding fluorescence spectra in the range of 400–750 nm under excitation at 980 nm. The Gd_2O_3:Yb^{3+}/Tm^{3+} UCNs exhibit three main upconversion emission bands in the visible spectrum, including a strong blue emission band at around 476 nm and two relatively weak red emission peaks centered at 653 and 695 nm. The Gd_2O_3:Yb^{3+}/Ho^{3+} UCNs have a strong green emission at 543 nm and a weak red emission at 667 nm, while the Gd_2O_3:Yb^{3+}/Er^{3+} UCNs exhibit a strong red emission at around 672 nm and two quite weak green emissions at ~528 and 547 nm. Interestingly, the red emission of Gd_2O_3:Yb^{3+}/

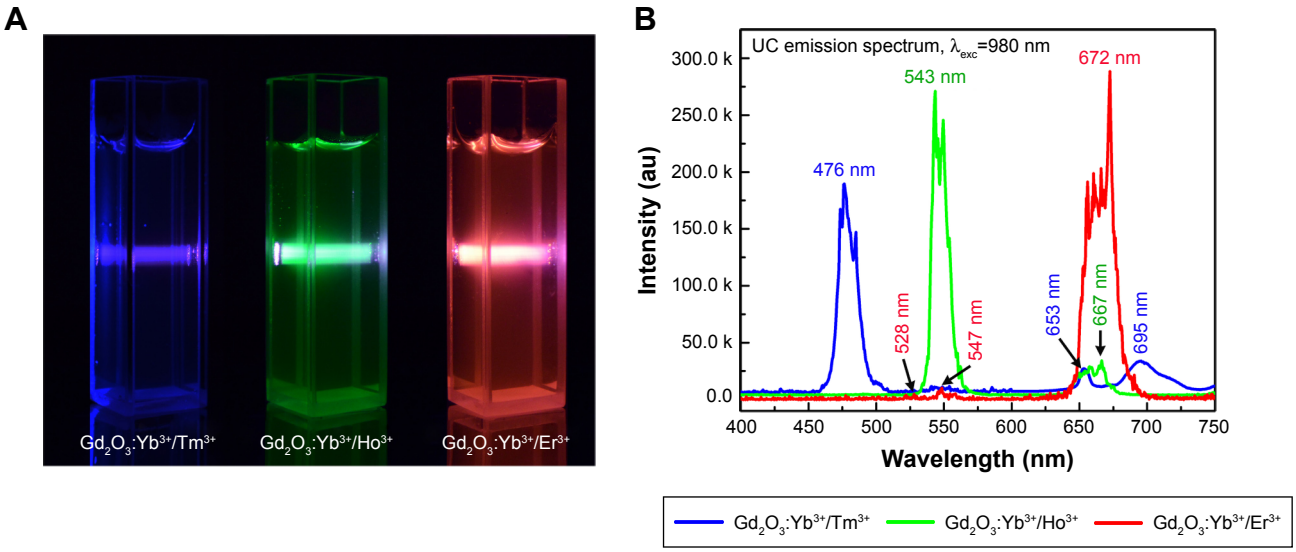

Figure 1 (**A**) Upconversion fluorescence images of the collected Gd_2O_3:Yb^{3+}/Ln^{3+} UCNs colloids under excitation at 980 nm, obtained using a digital camera without the use of a filter. (**B**) Room temperature upconversion emission spectra of Gd_2O_3:Yb^{3+}/Ln^{3+} UCNs under excitation at 980 nm.
Abbreviation: UCNs, upconversion nanoparticles.

Er^{3+} UCNs centered at 672 nm have a large red shift (over 10 nm) compared to the reported cubic counterpart.[32,42]

Tm^{3+}, Ho^{3+}, and Er^{3+} ions are the most common activators in UCNs and possess their own ladder-like energy levels, as shown in Figure S1. The intense blue and weak red emissions of Gd_2O_3:Yb^{3+}/Tm^{3+} UCNPs are assigned to the $^1G_4 \rightarrow {}^3H_6$ (476 nm), $^1G_4 \rightarrow {}^3H_5$ (653 nm), and $^3F_3 \rightarrow {}^3H_6$ (695 nm) transitions of Tm^{3+}. For Gd_2O_3:Yb^{3+}/Ho^{3+}, the peak near 543 nm is assigned to the $^5F_4/{}^5S_2 \rightarrow {}^5I_8$ transition of Ho^{3+}, and a weak emission in red region comes from $^5F_5 \rightarrow {}^5I_8$ (667 nm) transition. The intense red emission and two quite weak emissions in the green region of Gd_2O_3:Yb^{3+}/Er^{3+} UCNPs are assigned to the $^4F_{9/2} \rightarrow {}^4I_{15/2}$ (672 nm), $^4S_{3/2} \rightarrow {}^4I_{15/2}$ (547 nm) and $^2H_{11/2} \rightarrow {}^4I_{15/2}$ (528 nm) transitions of Er^{3+}, respectively. Thus, the different color fluorescence of the Gd_2O_3:Yb^{3+}/Ln^{3+} nanoparticles indicates that the Yb^{3+}, Tm^{3+}, Ho^{3+}, and Er^{3+} ions are successfully doped into the Gd_2O_3 matrix.

Structure, morphology, and component of Gd_2O_3:Yb^{3+}/Ln^{3+} UCNs

The crystal structures of the Gd_2O_3:Yb^{3+}/Ln^{3+} UCNs were characterized by XRD measurement. The collected UCNs colloids are dropped onto silicon substrates and evaporated for measurement. Figure 2 shows the XRD patterns of Gd_2O_3:Yb^{3+}/Ln^{3+} UCNs. The peaks of the UCNs match well to standard monoclinic Gd_2O_3 (PDF#42-1465). The strong narrow peaks are indicative of the high-quality crystallinity of the UCNs.

The typical TEM image, SAED pattern, HRTEM image, and size distribution histogram of the Gd_2O_3:Yb^{3+}/Er^{3+} UCNs are shown in Figure 3A–D. The results show that the as-prepared UCNs possess a nearly spherical shape with a wide-sized distribution. The corresponding size distribution histogram of the nanoparticles, which is fitted by the Gauss function, shows an average diameter of ~7.8 nm. However, the size calculated from XRD data by Scherrer equation is ~17.43 nm. Figure 3C shows the high resolution TEM (HRTEM) of UCNs. Clearly, small and large particles coexist and possess high crystallinity. In general, small nanoparticles usually make the peaks of XRD become wider, and even no peak can be detected for the ultrafine nanocrystals. We deduce that these high crystalline large nanoparticles may have much effect to enhance the signal of XRD measurement or large particles maybe picked in the XRD

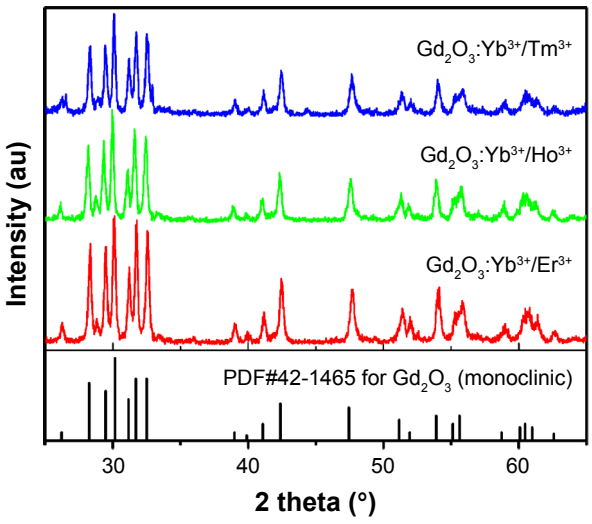

Figure 2 XRD patterns of the as-synthesized Gd_2O_3:Yb^{3+}/Ln^{3+} UCNs compared to PDF#42-1465 for monoclinic Gd_2O_3.
Abbreviations: UCNs, upconversion nanoparticles; XRD, X-ray diffractometer.

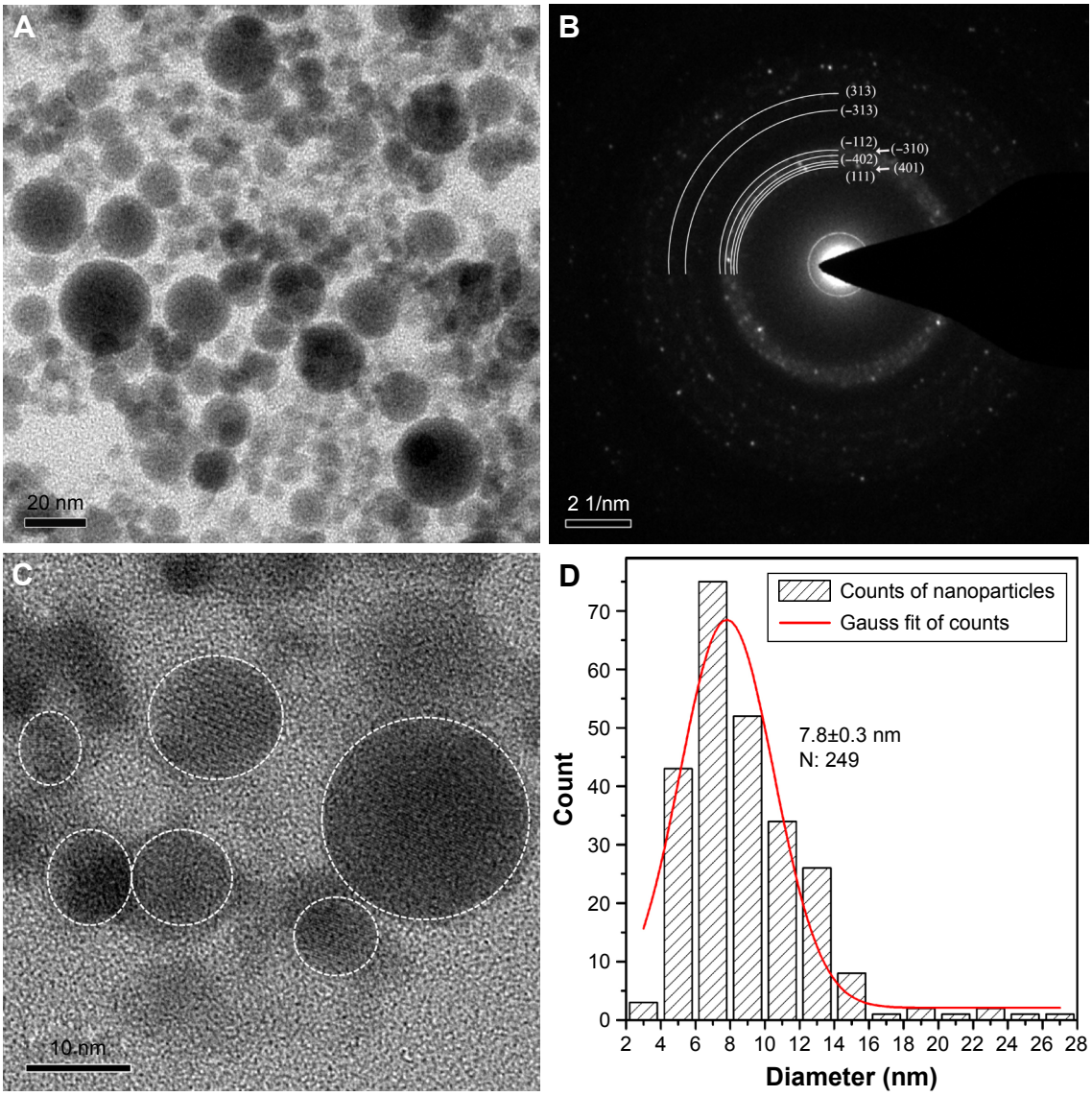

Figure 3 Typical TEM (**A**), SAED pattern (**B**), HRTEM (**C**), and size distribution histogram (**D**) of the Gd_2O_3:Yb^{3+}/Er^{3+} UCNs.
Abbreviations: HRTEM, high resolution TEM; SAED, selected area electron diffraction; TEM, transmission electron microscope; UCNs, upconversion nanoparticles; XRD, X-ray diffractometer.

measurement. The presence of large rings in the selected area electron diffraction pattern (Figure 3B) is further evidence of a polycrystalline structure. The ring spacings matched well with the crystallographic planes of monoclinic Gd_2O_3 (PDF#42-1465). Taking the Gd_2O_3:Yb^{3+}/Er^{3+} UCNs as an example, XPS was employed to confirm the components of the products. As shown in Figure S2, peaks at 1,220.4, 1,187.0, 184.0, and 169.5 eV denote $Gd3d_{3/2}$, $Gd3d_{5/2}$, Yb4d, and Er4d, respectively. The structure and component analyses demonstrate that Yb^{3+}/Er^{3+} ions are successfully co-doped into the Gd_2O_3 host matrix.

In vitro and in vivo MRI study

Samples were fed into the tubes in various concentrations between 0 and 0.1 mM for measurement. Figure 4A shows the T_1-weighted MR images of the Gd_2O_3:Yb^{3+}/Ln^{3+} UCNs and Gd-DTPA (clinical MRI contrast agent). The results reveal an enhanced brightness of the MRI signal with increasing UCNs concentration. For the same Gd concentration, the MRI using the UCNs as contrast agent is much brighter than those using Gd-DTPA, indicating that the Gd_2O_3:Yb^{3+}/Ln^{3+} nanoparticles possess better contrast enhancement than Gd-DTPA. The longitudinal relaxivity (r_1) value was measured to understand its effectiveness from a quantitative perspective. As shown in Figure 4B, R_1 ($1/T_1$) vs Gd concentration curves were plotted, and the slopes of the curves or r_1 were obtained for each sample. The r_1 values of Gd_2O_3:Yb^{3+}/Tm^{3+}, Gd_2O_3:Yb^{3+}/Ho^{3+}, and Gd_2O_3:Yb^{3+}/Er^{3+} UCNs are 13.23, 16.56, and 14.52 $s^{-1}mM^{-1}$, respectively. Note

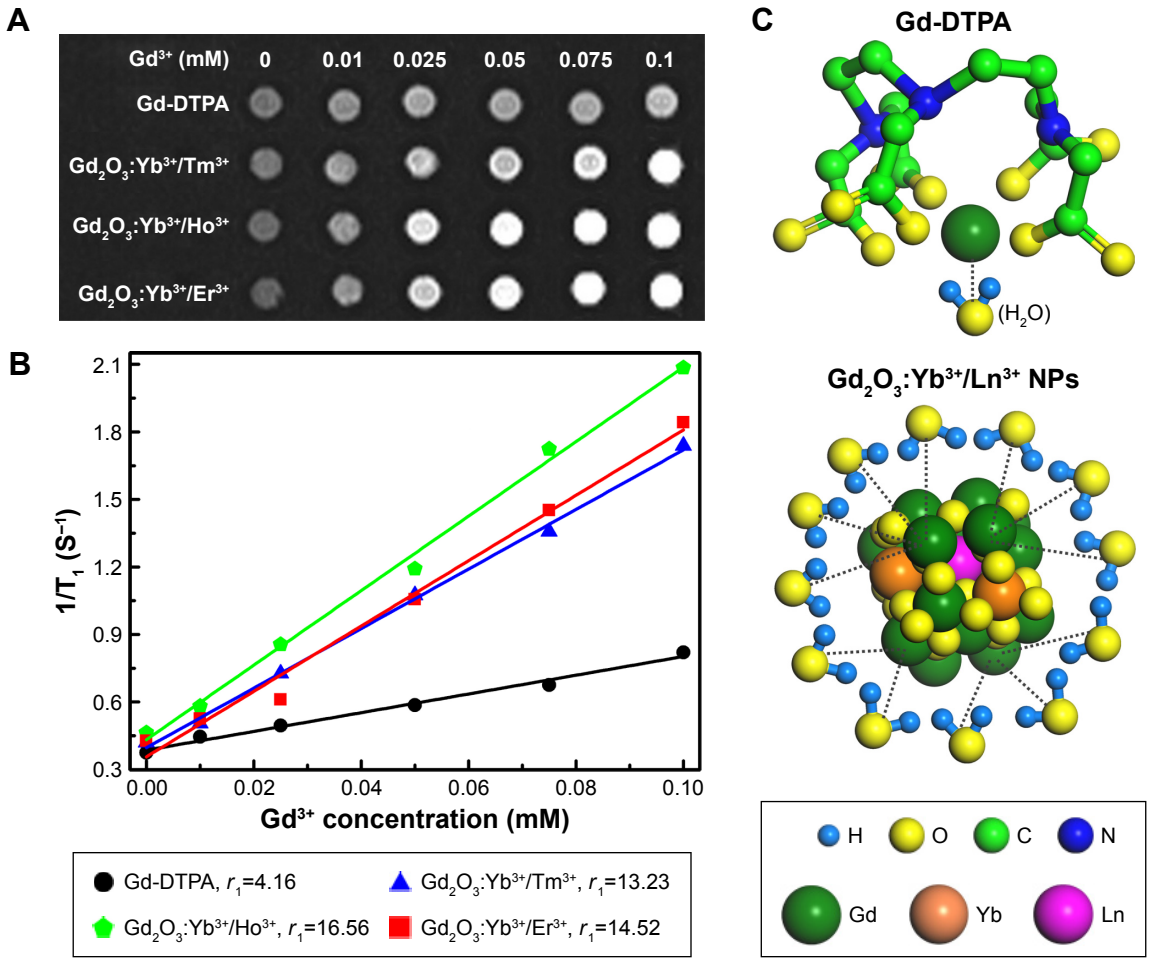

Figure 4 In vitro magnetic properties.
Notes: (A) In vitro T_1-weighted MRI of Gd_2O_3:Yb^{3+}/Ln^{3+} UCNs. (**B**) Plot of the relaxation rate ($1/T_1$) as a function of Gd^{3+} concentration, to provide the longitudinal relaxivity (r_1) of the Gd_2O_3:Yb^{3+}/Ln^{3+} UCNs. (**C**) Schematic illustration of the interaction between the contrast agents (Gd-DTPA and Gd_2O_3:Yb^{3+}/Ln^{3+} UCNs) and water.
Abbreviations: MRI, magnetic resonance imaging; NPs, nanoparticles; UCNs, upconversion nanoparticles.

that the r_1 values of Gd_2O_3:Yb^{3+}/Ln^{3+} UCNs are over three times higher than those of Gd-DTPA (4.16 $s^{-1}mM^{-1}$), which is consistent with the above contrast enhancement result.

Figure 4C illustrates the interaction between the contrast agents (Gd-DTPA and Gd_2O_3:Yb^{3+}/Ln^{3+} UCNs) and water. The r_1 value of the contrast agent is proportional to the water hydration number which directly corresponds to the unpaired electrons of Gd^{3+} ions.[43] The Gd^{3+} ions of Gd-DTPA can only offer one hydrate position since the other six unpaired electrons are coordinated by the chelates. However, a Gd^{3+} ion on the surface of the UCNs can offer all its seven unpaired electrons for water hydration, resulting in a higher r_1 value than Gd-DTPA. The T_1-weighted MR images of the NPC CNE-2 xenografted tumor (white arrow) in BALB/c nude mice are shown in Figure 5. T_1-weighted images in the axial orientations were obtained at 0, 5, 10, 15, 30, 45, 60, and 90 min after intravenous administration of the Gd_2O_3:Yb^{3+}/Er^{3+} nanoparticles and clearly show a high contrast enhancement of the tumor 30 min after injecting the Gd_2O_3:Yb^{3+}/Er^{3+} nanoparticles. Therefore, both the in vitro and in vivo MR imaging investigations indicate that the Gd_2O_3:Yb^{3+}/Er^{3+} nanoparticles may be a promising T_1-weighted MRI contrast agent for biomedical applications.

Confocal fluorescence imaging of live cells

The use of NIR light for the excitation of nanoparticles for molecular, cellular, and tissue imaging is very attractive in bioimaging applications owing to the lack of tissue damage and deep tissue penetrability.[15] To explore the feasibility of using the UCNs as biological fluorescence probes, we conducted in vitro biological experiments using a murine macrophage cells line (RAW 264.7 cells) incubated with Gd_2O_3:Yb^{3+}/Ln^{3+} UCNs. The cells were washed after incubation and imaged using a confocal laser fluorescence microscope operating at an excitation wavelength of 980 nm. As shown in Figures 6 and S3, blue, green, and red fluorescence can be observed from the cells incubated with the

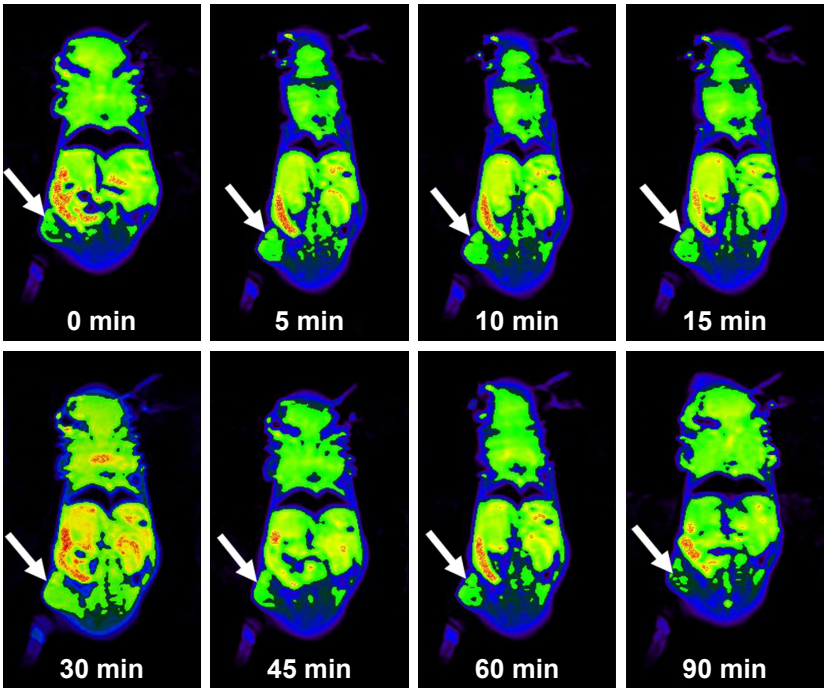

Figure 5 In vivo MRI of a NPC CNE-2 xenografted tumor after intravenous administration of the Gd_2O_3:Yb^{3+}/Er^{3+} UCNs (Gd^{3+}, 15 μmol/kg) at 0, 5, 10, 15, 30, 45, 60, and 90 min, respectively.
Abbreviations: MRI, magnetic resonance imaging; NPC, nasopharyngeal carcinoma; UCNs, upconversion nanoparticles; min, minutes.

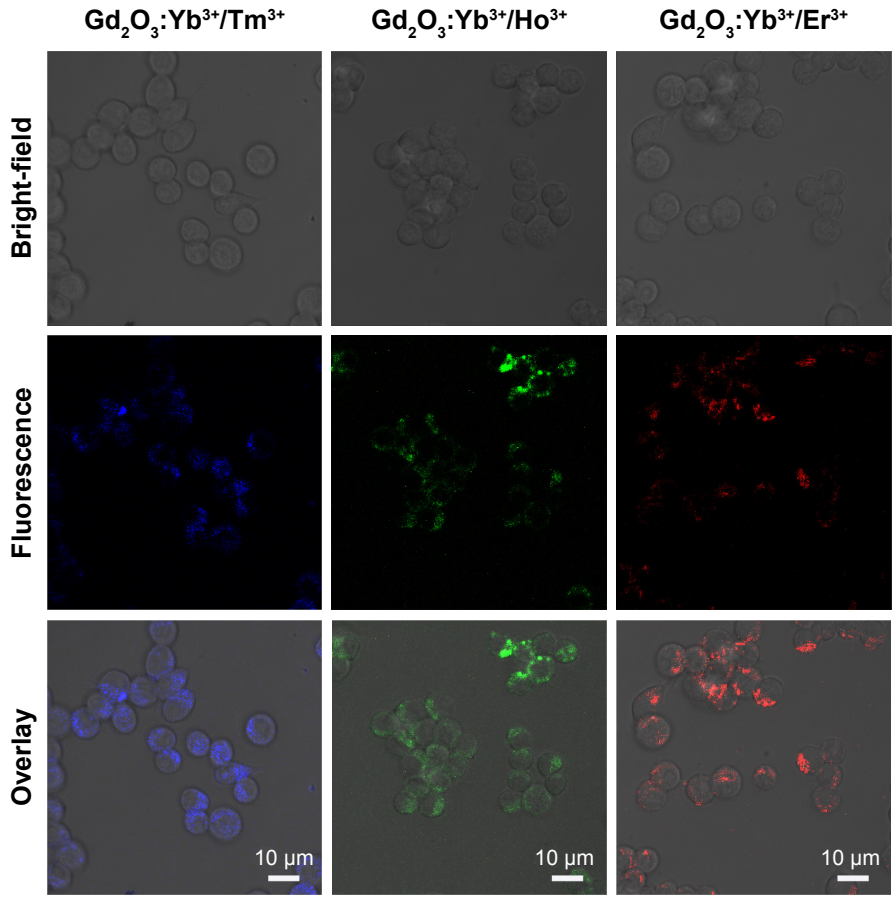

Figure 6 Confocal fluorescence images of RAW267.4 cells incubated with Gd_2O_3:Yb^{3+}/Ln^{3+} UCNs under excitation at 980 nm.
Abbreviation: UCNs, upconversion nanoparticles.

Gd_2O_3:Yb^{3+}/Tm^{3+}, Gd_2O_3:Yb^{3+}/Ho^{3+}, and Gd_2O_3:Yb^{3+}/Er^{3+} UCNs, respectively, with no autofluorescence found. The positions of the cells in the bright-field and the dark-field fluorescence imaging correlated well, and the fluorescence products were primarily located in the cell membrane and cytoplasm. The cells show good viability and morphology, suggesting that the products cause no significant damage to the cells. We also assessed the cells' viability after incubation with Gd_2O_3:Yb^{3+}/Ln^{3+} (Ln = Tm, Ho, and Er) UCNs (Figure S4). Clearly, there is no significant difference between the three kinds of nanoparticles and the negative control (PBS); the data showed that the cell toxicity of the three kinds of nanoparticles is satisfactory. This result indicates that the upconversion fluorescence emission of the UCNs is strong enough for live cell imaging and can be applied as potential fluorescence nanoprobes for in vivo imaging.

In vitro PDT

Cytotoxic singlet oxygen can result in cell death. Therefore, the ability to generate singlet oxygen is one of the crucial factors for effective PDT. Singlet oxygen production is generally monitored using DPBF, which reacts irreversibly with singlet oxygen causing a decrease of its characteristic absorption at ~410 nm.[39–41] As shown in Figure 7A, the combination of the UCNs (Gd_2O_3:Yb^{3+}/Er^{3+}) with PS (ZnPc) resulted in the highest rate of decomposition of the DPBF under NIR irradiation, and thus absorption of DPBF decreased exponentially

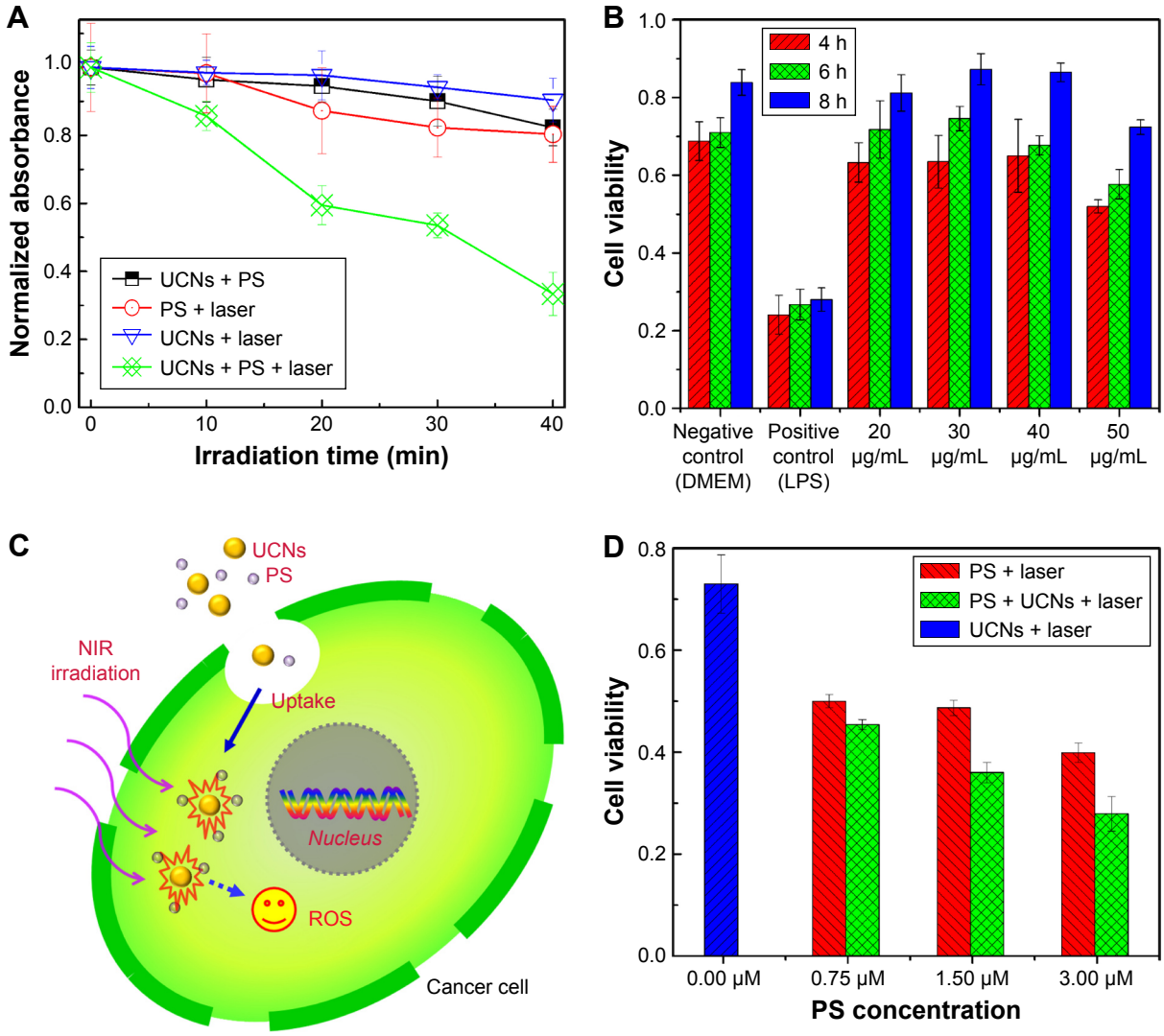

Figure 7 (**A**) Peak absorbance intensity of DPBF as a function of NIR irradiation time. (**B**) Cell viability of CNE2 cells after incubation with UCNs concentrations of 20, 30, 40, and 50 μg/mL for 4, 6, and 8 h. (**C**) Schematic illustration of the UCNs-based PDT treatment. (**D**) PDT experiment (with UCNs and different PS concentrations) and control experiment.

Abbreviations: DMEM, Dulbecco's Modified Eagle's Medium; DPBF, 1,3-diphenylisobenzofuran; h, hours; LPS, lipopolysaccharides; min, minutes; NIR, near-infrared; PDT, photodynamic therapy; PS, photosensitizer; UCNs, upconversion nanoparticles.

with increasing NIR irradiation time, confirming the efficient generation of singlet oxygen.

To understand the effects of PDT, the viability of cells containing the combination of UCNs and PS under NIR irradiation was studied. First, the viability of CNE2 cells after incubation with UCNs concentrations of 20, 30, 40, and 50 μg/mL for 4, 6, and 8 h was determined by MTT assay. As shown in Figure 7B, the UCNs have no significant intrinsic toxicity effect on the cells' survival. Then, the viability of CNE2 cells containing Gd-based UCNs (Gd_2O_3:Yb^{3+}/Er^{3+}, 40 μg/mL) and the ZnPc (0.75, 1.5, and 3 μM) under NIR irradiation was measured and compared to the control experiment. The UCNs-based PDT treatment is schematically illustrated in Figure 7C. The NIR irradiation of the UCNs emitted red light (~672 nm), excited the ZnPc (maximum absorption peak at ~670 nm), which then generated singlet oxygen to kill the cancer cells. The results shown in Figure 7D demonstrate that the cells' viabilities of samples containing combinations of UCNs and ZnPc are lower than their control groups, meaning that this NIR-induced PDT can inhibit the proliferation of cancer cells.

Conclusion

In summary, magnetic and fluorescent lanthanide-doped Gd_2O_3 UCNs imaging have been fabricated and can simultaneously achieve MR/UCL dual-modal imaging and PDT. As an MRI contrast agent, the products show a high longitudinal relaxivity (r_1) value and T_1-weighted contrast enhancement of xenografted tumors in mice. As UCL imaging nanoprobes, the products exhibit bright luminescence under NIR irradiation. Moreover, upon NIR excitation, PDT can be achieved by the combination of the UCNs and the PS ZnPc. We anticipate that the magnetic and fluorescent lanthanide-doped Gd_2O_3 UCNs will be a highly attractive addition to the theranostic platform, and promote the development of "detect-to-treat" strategies or imaging-guided therapy of cancer.

Acknowledgments

This work was supported by the National Basic Research Program of China (2014CB931700), the National Natural Science Foundation of China (grant nos 81471787, 61471401, 81471711, 81271622, and 11274394), the National Science Foundation for Young Scholars of China (grant no 81401462), Natural Science Foundation of Guangdong, China (no 2014A030311036), and State Key Laboratory of Optoelectronic Materials and Technologies (Sun Yat-Sen University; no OEMT-2015-KF-03).

Author contributions

JL, LH, XT, XC, YS, and FX: experimental work. DC and LL: project planning. All authors contributed toward data analysis, drafting and revising the paper and agree to be accountable for all aspects of the work.

Disclosure

The authors report no conflicts of interest in this work.

References

1. Lucky SS, Soo KC, Zhang Y. Nanoparticles in photodynamic therapy. *Chem Rev*. 2015;115(4):1990–2042.
2. Chen Z, Li Z, Wang J, et al. A multi-synergistic platform for sequential irradiation-activated high-performance apoptotic cancer therapy. *Adv Funct Mater*. 2013;24(4):522–529.
3. Bonnett R. Photosensitizers of the porphyrin and phthalocyanine series for photodynamic therapy. *Chem Soc Rev*. 1995;24(1):19–33.
4. Rosenkranz AA, Jans DA, Sobolev AS. Targeted intracellular delivery of photosensitizers to enhance photodynamic efficiency. *Immunol Cell Biol*. 2000;78(4):452–464.
5. Wei W, Zhang Y, Chen R, et al. Cross relaxation induced pure red upconversion in activator- and sensitizer-rich lanthanide nanoparticles. *Chem Mater*. 2014;26(18):5183–5186.
6. Chen GY, Shen J, Ohulchanskyy TY, et al. (α-$NaYbF_4$:Tm^{3+})/CaF_2 core/shell nanoparticles with efficient near-infrared to near-infrared upconversion for high-contrast deep tissue bioimaging. *ACS Nano*. 2012;6(9):8280–8287.
7. Li RB, Ji ZX, Dong JY, et al. Enhancing the imaging and biosafety of upconversion nanoparticles through phosphonate coating. *ACS Nano*. 2015;9(3):3293–3306.
8. Auzel F. Upconversion and anti-stokes processes with f and d ions in solids. *Chem Rev*. 2004;104(1):139–174.
9. Wang L, Yan R, Huo Z, et al. Fluorescence resonant energy transfer biosensor based on upconversion-luminescent nanoparticles. *Angew Chem Int Ed Engl*. 2005;44(37):6054–6057.
10. Haase M, Schäfer H. Upconverting nanoparticles. *Angew Chem Int Ed Engl*. 2011;50(26):5808–5829.
11. Zhang P, Steelant W, Kumar M, Scholfield M. Versatile photosensitizers for photodynamic therapy at infrared excitation. *J Am Chem Soc*. 2007;129(15):4526–4527.
12. Idris NM, Gnanasammandhan MK, Zhang J, Ho PC, Mahendran R, Zhang Y. In vivo photodynamic therapy using upconversion nanoparticles as remote-controlled nanotransducers. *Nat Med*. 2012;18(10):1580–1585.
13. Chatterjee DK, Yong Z. Upconverting nanoparticles as nanotransducers for photodynamic therapy in cancer cells. *Nanomedicine*. 2008;3(1):73–82.
14. Wang M, Chen Z, Zheng W, et al. Lanthanide-doped upconversion nanoparticles electrostatically coupled with photosensitizers for near-infrared-triggered photodynamic therapy. *Nanoscale*. 2014;6(14):8274–8282.
15. Chen G, Qiu H, Prasad PN, Chen X. Upconversion nanoparticles: design, nanochemistry, and applications in theranostics. *Chem Rev*. 2014;114(10):5161–5214.
16. Cui S, Chen H, Zhu H, et al. Amphiphilic chitosan modified upconversion nanoparticles for in vivo photodynamic therapy induced by near-infrared light. *J Mater Chem*. 2012;22(11):4861–4873.
17. Guo HC, Qian HS, Idris NM, Zhang Y. Singlet oxygen-induced apoptosis of cancer cells using upconversion fluorescent nanoparticles as a carrier of photosensitizer. *Nanomedicine*. 2010;6(3):486–495.
18. Qian HS, Guo HC, Ho PC, Mahendran R, Zhang Y. Mesoporous-silica-coated up-conversion fluorescent nanoparticles for photodynamic therapy. *Small*. 2009;5(20):2285–2290.

19. Liu K, Liu X, Zeng Q, et al. Covalently assembled NIR nanoplatform for simultaneous fluorescence imaging and photodynamic therapy of cancer cells. *ACS Nano*. 2012;6(5):4054–4062.
20. Jin S, Zhou L, Gu Z, et al. A new near infrared photosensitizing nanoplatform containing blue-emitting up-conversion nanoparticles and hypocrellin A for photodynamic therapy of cancer cells. *Nanoscale*. 2013;5(23):11910–11918.
21. Park YI, Kim HM, Kim JH, et al. Theranostic probe based on lanthanide-doped nanoparticles for simultaneous in vivo dual-modal imaging and photodynamic therapy. *Adv Mater*. 2012;24(42):5755–5761.
22. Qiao XF, Zhou JC, Xiao JW, Wang YF, Sun LD, Yan CH. Triple-functional core-shell structured upconversion luminescent nanoparticles covalently grafted with photosensitizer for luminescent, magnetic resonance imaging and photodynamic therapy in vitro. *Nanoscale*. 2012; 4(15):4611–4623.
23. Zhao Z, Han Y, Lin C, et al. Multifunctional core–shell upconverting nanoparticles for imaging and photodynamic therapy of liver cancer cells. *Chem Asian J*. 2012;7(4):830–837.
24. Chen Q, Wang C, Cheng L, He W, Cheng Z, Liu Z. Protein modified upconversion nanoparticles for imaging-guided combined photothermal and photodynamic therapy. *Biomaterials*. 2014;35(9):2915–2923.
25. Zheng K, Zhang D, Zhao D, Liu N, Shi F, Qin W. Bright white upconversion emission from Yb^{3+}, Er^{3+}, and Tm^{3+}-codoped Gd_2O_3 nanotubes. *Phys Chem Chem Phys*. 2010;12(27):7620–7625.
26. Chen GY, Zhang YG, Somesfalean G, Zhang ZG, Sun Q, Wang FP. Two-color upconversion in rare-earth-ion-doped ZrO_2 nanocrystals. *Appl Phys Lett*. 2006;89(16):163105.
27. Chen GY, Liu Y, Zhang YG, et al. Bright white upconversion luminescence in rare-earth-ion-doped Y_2O_3 nanocrystals. *Appl Phys Lett*. 2007; 91(13):3103.
28. Park JY, Baek MJ, Choi ES, et al. Paramagnetic ultrasmall gadolinium oxide nanoparticles as advanced T_1 MRI contrast agent: account for large longitudinal relaxivity, optimal particle diameter, and in vivo T_1 MR images. *ACS Nano*. 2009;3(11):3663–3669.
29. Klasson A, Ahrén M, Hellqvist E, et al. Positive MRI contrast enhancement in THP-1 cells with Gd_2O_3 nanoparticles. *Contrast Media Mol Imaging*. 2008;3(3):106–111.
30. Ahrén M, Selegard L, Klasson A, et al. Synthesis and characterization of PEGylated Gd_2O_3 nanoparticles for MRI contrast enhancement. *Langmuir*. 2010;26(8):5753–5762.
31. Zhou L, Gu Z, Liu X, et al. Size-tunable synthesis of lanthanide-doped Gd_2O_3 nanoparticles and their applications for optical and magnetic resonance imaging. *J Mater Chem*. 2012;22(3):966–974.
32. Liu Z, Pu F, Huang S, Yuan Q, Ren J, Qu X. Long-circulating Gd_2O_3:Yb^{3+}, Er^{3+} up-conversion nanoprobes as high-performance contrast agents for multi-modality imaging. *Biomaterials*. 2013;34(6):1712–1721.
33. Chen F, Chen M, Yang C, et al. Terbium-doped gadolinium oxide nanoparticles prepared by laser ablation in liquid for use as a fluorescence and magnetic resonance imaging dual-modal contrast agent. *Phys Chem Chem Phys*. 2015;17(2):1189–1196.
34. Liu J, Tian XM, Luo NQ, et al. Sub-10 nm monoclinic Gd_2O_3:Eu^{3+} nanoparticles as dual-modal nanoprobes for magnetic resonance and fluorescence imaging. *Langmuir*. 2014;30(43):13005–13013.
35. Luo N, Yang C, Tian X, et al. A general top-down approach to synthesize rare earth doped-Gd_2O_3 nanocrystals as dualmodal contrast agents. *J Mater Chem B*. 2014;2(35):5891–5897.
36. Liu J, Deng H, Huang Z, Chen D, Shao Y. Phonon-assisted energy back transfer-induced multicolor upconversion emission of Gd_2O_3:Yb^{3+}/Er^{3+} nanoparticles under near-infrared excitation. *Phys Chem Chem Phys*. 2015;17(23):15412–15418.
37. Yang GW. Laser ablation in liquids: applications in the synthesis of nanocrystals. *Prog Mater Sci*. 2007;52(4):648–698.
38. Yan Z, Chrisey DB. Pulsed laser ablation in liquid for micro-/nanostructure generation. *J Photochem Photobiol C Photochem Rev*. 2012; 13(3):204–223.
39. Fujii M, Usui M, Hayashi S, et al. Singlet oxygen formation by porous Si in solution. *Phys Status Solidi A*. 2005;202(8):1385–1389.
40. Mukai K, Ouchi A, Takahashi S, et al. Development of singlet oxygen absorption capacity (SOAC) assay method. 3. measurements of the SOAC values for phenolic antioxidants. *J Agric Food Chem*. 2012; 60(32):7905–7916.
41. Ikehata T, Onodera Y, Nunokawa T, et al. Photodynamic therapy using upconversion nanoparticles prepared by laser ablation in liquid. *Appl Surf Sci*. 2015;348:54–59.
42. Lei Y, Song H, Yang L, et al. Upconversion luminescence, intensity saturation effect, and thermal effect in Gd_2O_3: Er^3, Yb^{3+} nanowires. *J Chem Phys*. 2005;123(17):174710.
43. Caravan P. Strategies for increasing the sensitivity of gadolinium based MRI contrast agents. *Chem Soc Rev*. 2006;35(6):512–523.

Supplementary materials

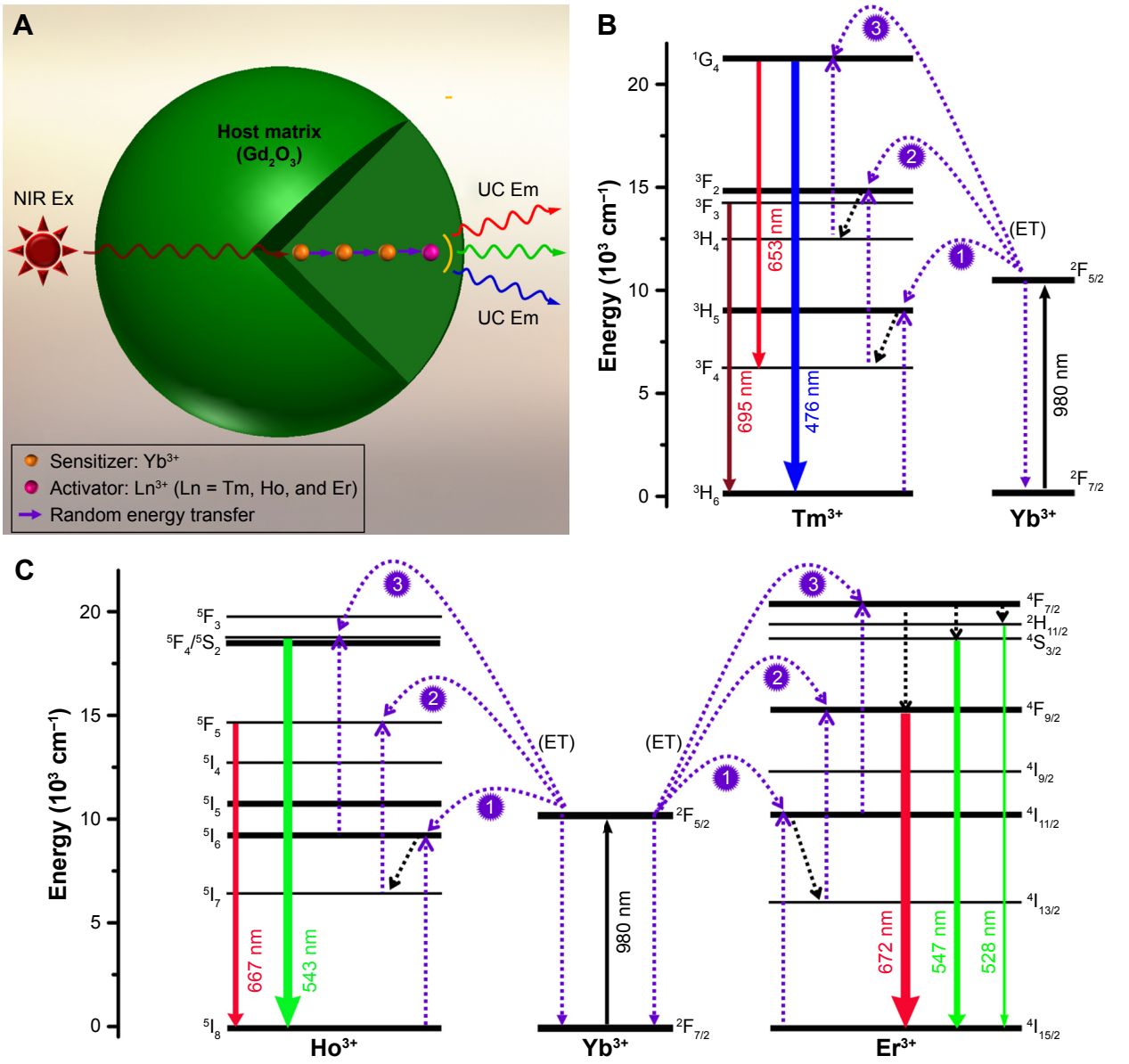

Figure S1 Schematic illustration of the UC emission process (**A**), and the proposed UC mechanism schemes (**B**, **C**) of the Gd_2O_3:Yb^{3+}/Ln^{3+} (Ln = Tm, Ho, and Er) UCNs.
Abbreviations: NIR, near-infrared; UC, upconversion; ET, energy transfer; Ex, excitation; Em, emission.

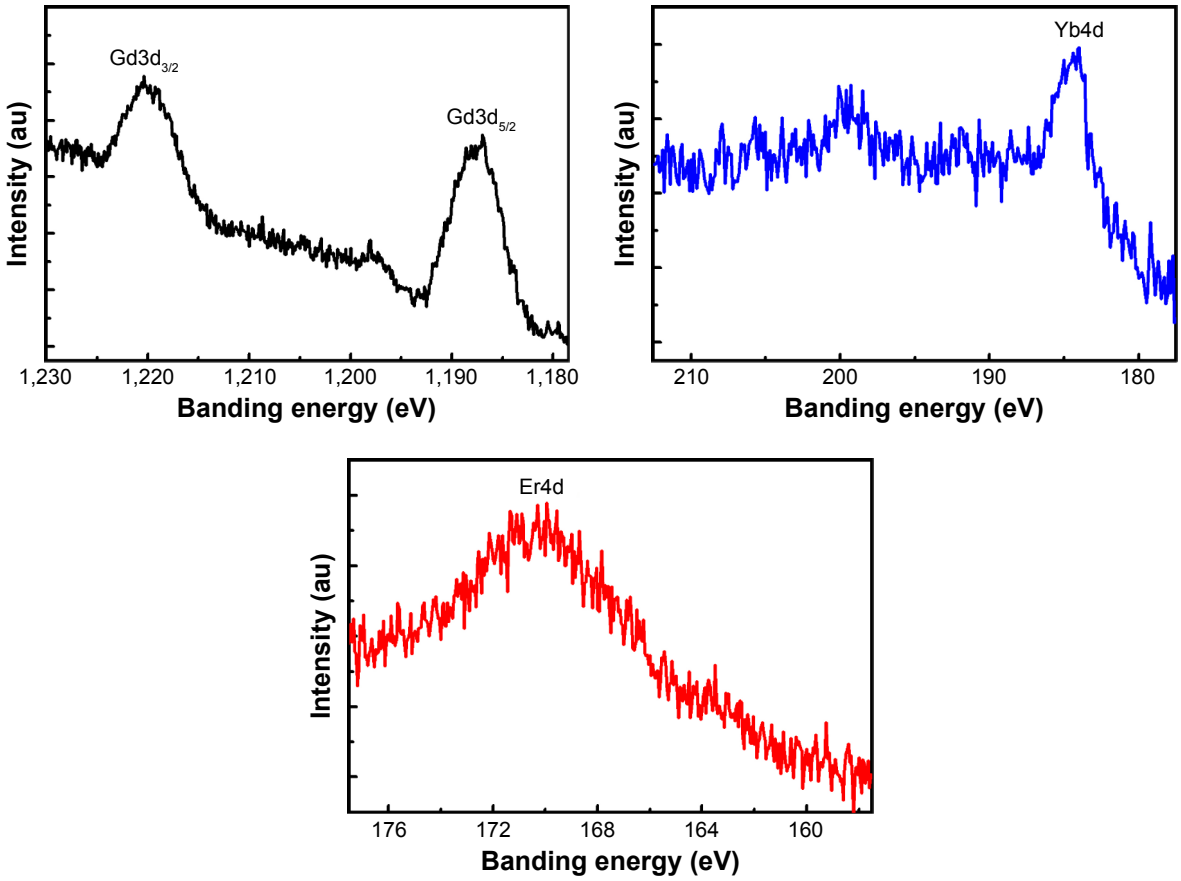

Figure S2 Gd3d, Yb4d, and Er4d XPS spectra of Gd_2O_3:Yb^{3+}/Er^{3+} UCNs.

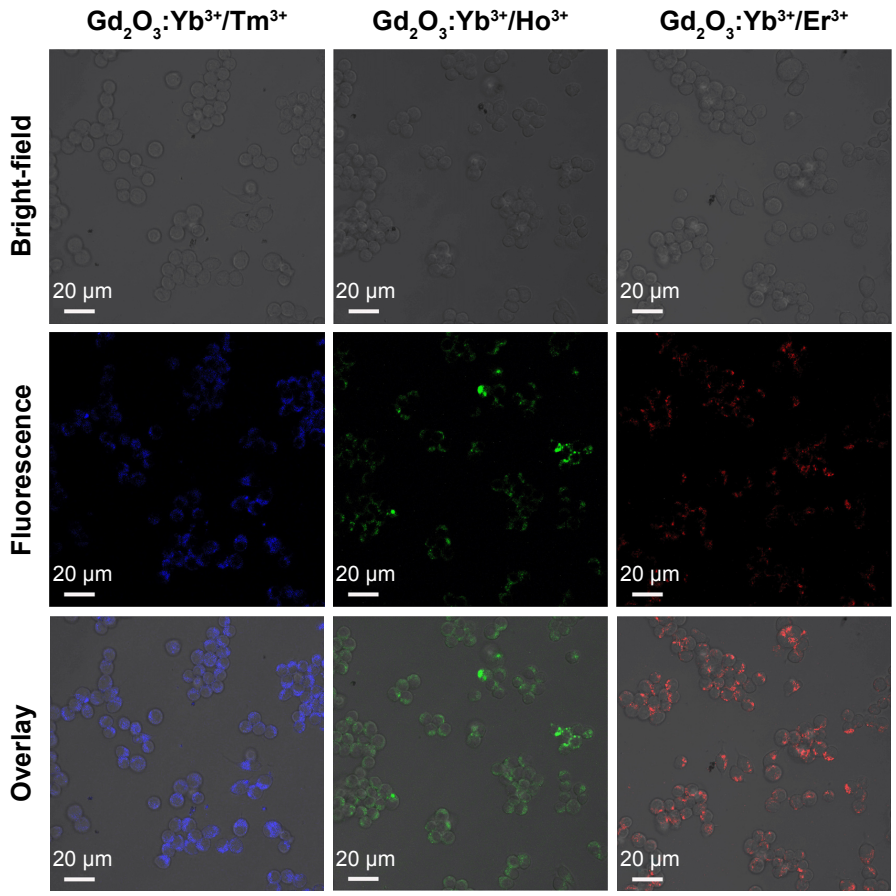

Figure S3 Confocal fluorescence images of Raw267.4 cells incubated with Gd_2O_3:Yb^{3+}/Ln^{3+} UCNs.

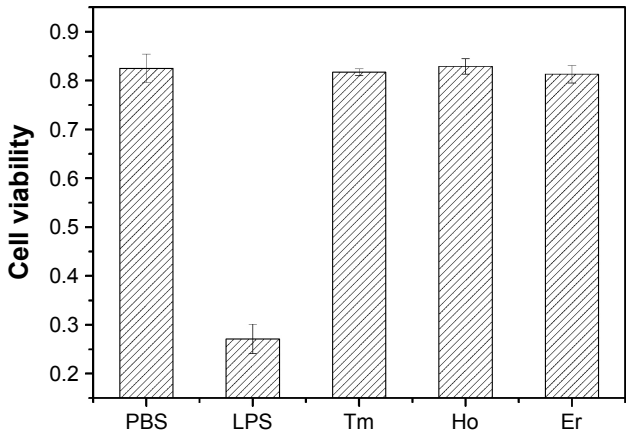

Figure S4 Cells viability of Raw267.4 cells incubated with Gd_2O_3:Yb^{3+}/Ln^{3+} (Ln = Tm, Ho, and Er) UCNs (20μg/mL at 2 hours.
Abbreviations: LPS, lipopolysaccharides; PBS, phosphate-buffered saline.